Atmos. Chem. Phys. Discuss., 6, 5095–5136, 2006
www.atmos-chem-phys-discuss.net/6/5095/2006/

Atmospheric Chemistry and Physics Discussions

Radiative forcing by aerosols as derived from the AeroCom present-day and pre-industrial simulations

M. Schulz[1], C. Textor[1], S. Kinne[2], Y. Balkanski[1], S. Bauer[3], T. Berntsen[4], T. Berglen[4], O. Boucher[5,11], F. Dentener[6], S. Guibert[1], I. S. A. Isaksen[4], T. Iversen[4], D. Koch[3], A. Kirkevåg[4], X. Liu[7], V. Montanaro[8], G. Myhre[4], J. E. Penner[7], G. Pitari[8], S. Reddy[9], Ø. Seland[4], P. Stier[2], and T. Takemura[10]

[1]Laboratoire des Sciences du Climat et de l'Environnement, CEA-CNRS, Gif-sur-Yvette, France
[2]Max-Planck-Institut für Meteorologie, Centre for Marine and Atmospheric Sciences (ZMAW), Hamburg, Germany
[3]Columbia University, GISS, New York, USA
[4]University of Oslo, Department of Geosciences, Oslo, Norway
[5]Hadley Centre, Met Office, Exeter, United Kingdom
[6]EC, Joint Research Centre, Institute for Environment and Sustainability, Climate Change Unit, Italy
[7]Department of Atmospheric, Oceanic and Space Sciences, University of Michigan, Ann Arbor, MI, USA
[8]Dipartimento di Fisica, Università degli Studi L'Aquila, Coppito, Italy

[9]NOAA, Geophysical Fluid Dynamics Laboratory, Princeton, New Jersey, USA
[10]Research Institute for Apllied mechanics, Kyushu University, Fukuoka, Japan
[11]Laboratoire d'Optique Atmospherique, Université des Sciences et Technologies de Lille, CNRS, Villeneuve d'Ascq, France

Received: 25 April 2006 – Accepted: 11 May 2006 – Published: 22 June 2006

Correspondence to: M. Schulz (michael.schulz@cea.fr)

Abstract

Nine different global models with detailed aerosol modules have independently produced instantaneous direct radiative forcing due to anthropogenic aerosols. The anthropogenic impact is derived from the difference of two model simulations with identically prescribed aerosol emissions, one for present-day and one for pre-industrial conditions. The difference in the energy budget at the top of the atmosphere (ToA) yields a new harmonized estimate for the aerosol direct radiative forcing (RF) under all-sky conditions. On a global annual basis RF is $-0.2\,\mathrm{Wm}^{-2}$, with a standard deviation of $\pm 0.2\,\mathrm{Wm}^{-2}$. Anthropogenic nitrate and dust are not included in this estimate. No model shows a significant positive all-sky RF. The corresponding clear-sky RF is $-0.6\,\mathrm{Wm}^{-2}$. The cloud-sky RF was derived based on all-sky and clear-sky RF and modelled cloud cover. It was significantly different from zero and ranged between -0.16 and $+0.34\,\mathrm{Wm}^{-2}$. A sensitivity analysis shows that the total aerosol RF is influenced by considerable diversity in simulated residence times, mass extinction coefficients and most importantly forcing efficiencies (forcing per unit optical depth). Forcing efficiency differences among models explain most of the variability, mainly because all-sky forcing estimates require proper representation of cloud fields and the correct relative altitude placement between absorbing aerosol and clouds. The analysis of the sulphate RF shows that differences in sulphate residence times are compensated by opposite mass extinction coefficients. This is explained by more sulphate particle humidity growth and thus higher extinction in models with short-lived sulphate present at lower altitude and vice versa. Solar absorption within the atmospheric column is estimated at $+0.85\,\mathrm{Wm}^{-2}$. The local annual average maxima of atmospheric forcing exceed $+5\,\mathrm{Wm}^{-2}$ confirming the regional character of aerosol impacts on climate. The annual average surface forcing is $-1.03\,\mathrm{Wm}^{-2}$.

1 Introduction

Anthropogenic aerosols modify the Earth radiation budget such that flux changes can be observed by satellites (Bellouin et al., 2005). Their increased presence since pre-industrial times is suspected to have partly offset global warming in the 20th century (Charlson et al., 1992). This in turn would be responsible for additional climate warming if aerosols were removed in the future through abatement of aerosol related air pollution (Anderson et al., 2003). There is also a suggestion that aerosol forcing has an important regional impact on weather and climate (Menon et al., 2002). Reduced incoming radiation observed at surface level, called global dimming, was associated with the effect of aerosols (Liepert et al., 2004; Stanhill and Cohen, 2001).

The need to integrate the aerosol effects on a global scale has given rise in recent years to the development of models, in which aerosol modules gained considerable complexity (Ghan, 2001; Liao et al., 2004; Martin et al., 2004; Stier et al., 2005). However, individual models still suffer from technical difficulties in representing the aerosol physics in a sufficiently coherent and complex way so as to reproduce all aspects observed with a wide range of aerosol instruments. The model inter-comparison within the framework of the AeroCom initiative (http://nansen.ipsl.jussieu.fr/AEROCOM/) has revealed important differences in describing the aerosol life cycle at all stages from emission to optical properties (Kinne et al., 2006; Textor et al., 2006).

Here we present the results of a joint study of AeroCom models with the aim of deriving a state-of-the-art best guess for the direct radiative forcing (RF) attributable to anthropogenic aerosol. With the additional diagnostics available in AeroCom we also aim to analyze the differences in RF between models. Note, this RF does not include contributions of aerosol induced changes to clouds and the hydrological cycle, the indirect forcing. The RF collected here lacks the eventual contributions from anthropogenic nitrate and dust. Two experiments were performed by each of the models based on predefined emission datasets assumed to be representative for pre-industrial times at about 1750 ("AeroCom PRE") and for the year 2000 ("AeroCom B"). The differ-

ence in radiative energy balance between both experiments defines the impact due to anthropogenic aerosol. This definition also captures the effect of any non-linear aerosol dynamics, when anthropogenic aerosol interacts with the natural aerosol background. We note here that in this study we prescribed the emissions: the uncertainties in the emission datasets would add to the over-all uncertainty of our RF calculation.

2 Model simulations

2.1 Experimental setup

The analysis of the model results in this study builds on an open call to aerosol modelling groups to run specific simulations with prescribed aerosol emissions for current (AeroCom B) and pre-industrial conditions (AeroCom PRE). Groups were asked to provide output according to a protocol available on the AeroCom website (http://nansen.ipsl.jussieu.fr/AEROCOM/protocol.html). Nine (of the sixteen) AeroCom models contributed their RF results. Table 1 lists the models, their abbreviations and references to publications that provide more detail. Additional information on the model behavior with respect to the aerosol life cycle and optical properties is available in the initial AeroCom overview papers (Kinne et al., 2006; Textor et al., 2006). Initial checks of the received output were conducted via an interactive website open to the public (http://nansen.ipsl.jussieu.fr/AEROCOM/data.html). The parameters gathered comprise daily values for RF at the top of the atmosphere and at the surface, plus associated data on aerosol properties (mass loading, optical depth, size, absorption, single scattering albedo, altitude, component mass extinction efficiencies) and on environmental properties (solar surface albedo and cloud distribution). For both experiments AeroCom B and AeroCom PRE the modelers were asked to use a priori the analyzed meteorological fields for the year 2000 to either drive or nudge their model. This was done to obtain results corresponding to the AeroCom A experiment, where modelers used their usual emissions, and which were analyzed in the above mentioned overview

publications. The two participating models without nudging capability (UIO-GCM and ULAQ) established climatological means based on a 5-year simulation after a spin-up period of one year.

In addition to individual model results we also present data from an average AeroCom model, constructed from the outputs of the nine models. The original data were re-gridded by interpolation to a common grid of horizontal resolution of 1×1 degree latitude/longitude. A local diversity diagnostic at any grid point is calculated as the standard deviation from the values of the nine models.

2.2 AeroCom emission datasets

Inventories for global emissions of aerosol and pre-cursor gases for the years 2000 (current conditions) and 1750 (pre-industrial conditions) were established based on available data in 2003. All emissions data-sets are available via a file transfer site at the Joint Research Center (JRC), Italy: ftp://ftp.ei.jrc.it/pub/Aerocom/. Here, we give a very brief description and the reader is referred to (Dentener et al., 2006) for more detailed information. Dust, sea-salt, sulphur components and carbonaceous aerosol emissions are provided at a spatial resolution of $1^{\circ}\times1^{\circ}$. Temporal resolution ranges from daily for dust, sea salt and DMS to yearly for the remaining constituents. The injection altitudes and the size of the injected particles of emissions are prescribed. Aerosol emissions are categorized by its origin into “natural” and “anthropogenically modified”. Natural emissions of sea-salt, dust, DMS, secondary organic aerosol and volcanic activity are assumed identical for current and pre-industrial conditions. Anthropogenically modified emissions consider contributions to sulphur (S), Particulate Organic Matter (POM) and Black (or elementary) Carbon (BC) from large scale wild-land fires (partly natural), bio fuel burning and fossil fuel burning. For pre-industrial times contributions from wild-land fires (open burning) and biofuel emissions are reduced and fossil fuels emissions are ignored. In summary we assume anthropogenic emissions for black carbon of 6.32 Tg/year, for particulate organic matter of 32.5 Tg/year and for sulphur dioxide of

100.9 TG-SO2/year.

2.3 Model simulation of the anthropogenic components and forcing

The RF calculations analysed in this study involve nine different model environments with respect to the complexity of aerosol module and associated global circulation model. While the reader is encouraged to explore publications describing the individual models (see Table 1) together with the initial AeroCom papers from (Textor et al., 2006) and Kinne et al. (2006), we consider it necessary here to document some of the differences in the RF calculation.

RF is defined as "*the change in net (down minus up) irradiance (solar plus long-wave; in Wm^{-2}) at the tropopause AFTER allowing for stratospheric temperatures to readjust to radiative equilibrium, but with surface and tropospheric temperatures and state held fixed at the unperturbed values*", which is exerted by the introduction of a perturbing agent (Ramaswamy et al., 2001). For most aerosol constituents stratospheric adjustment has little effect on the RF, and the instantaneous RF at the top of the atmosphere (ToA) can be substituted for the stratospheric-adjusted RF. AeroCom RF results refer to ToA-RF. With respect to the flux perturbation by the anthropogenic aerosol we suggest here that the unperturbed state is characterized by experiment AeroCom-PRE. The analysis of the RF differences between models requires that we also retrieve the anthropogenic perturbation for several other parameters, such as load and optical depth. This has been obtained by subtracting AeroCom-PRE from AeroCom-B simulation results. Since these are the only useful parameter values to be compared to RF we omit for simplicity in the remainder the specification "anthropogenic" for the other parameters. "Load" thus refers just to the anthropogenic load, if not mentioned otherwise.

Note that the RF derived from the AeroCom simulations does not include anthropogenic nitrate and dust, since they are not considered in the AeroCom emission database. The omission of anthropogenic dust, of which the sources are very uncertain, simplifies the RF calculations in that only solar broadband flux changes need to be considered. Recent work (by Reddy et al., 2005a) suggests that significant flux

changes in the infrared part of the spectrum occur only in the presence of mineral dust. RF results reported here are for the shortwave spectrum only.

A conceptual difference among models in obtaining RF of the anthropogenic aerosol and its components is the choice of the unperturbed reference state. Internal mixing and other interactions between aerosol components affect size distribution and hygroscopicity and result in interdependencies between e.g. the sulphate RF and the black carbon RF. For the total aerosol RF a reference state with natural background aerosol is preferred over a no-aerosol reference. The experimental set-up ("B"–"PRE") establishes this type of a natural aerosol reference, and it guarantees comparability among models for the total anthropogenic (direct aerosol) impact. However, for individual aerosol component RF calculation the methodology differs. One way would be to isolate the perturbation due to a single component by an additional experiment, in addition to "B" and "PRE", where the target component is absent. MPI_HAM simulations refer to three experiments on top of a present day reference case to identify separately the RF of sulphate, fossil fuel carbonaceous aerosol and total aerosol. Another solution was chosen in UIO_GCM where the contribution from BC, POM, BC+POM and sulphate are removed in two more experiments per species from both present day and pre-industrial simulations. RF is then the difference between two pairs of simulation: RF_x=(B-PRE)–B_{-x}–PRE_{-x}). Most models did not try to account for non-linear effects and computed the RF of individual components from aerosol component fields established in experiment B against the Reference case PRE. It is beyond the scope of this paper and not documented in the AeroCom dataset how the non-linear effects of aerosol mixing influence the RF results. The consequences of the different ways of describing a reference state are difficult to estimate without dedicated experiments in a single model. The results summarised here involve both model diversity with respect to aerosol properties and RF calculation concept.

Finally, for completeness and also comparability with published data, we document here deviations from the general methodology described above or from work in publications cited e.g. in Table 1. Note that these deviations are model specific and due

rather to technical problems when setting up the AeroCom experiment. The following is thus more a listing and consequences for this study are thought to be small: Several models had locally negative values for aerosol mass and aerosol optical thickness. Since the overall average for these values was negligible they were simply removed from consideration. Deviating from AeroCom experiment A the SPRINTARS model treated black carbon (BC) and particulate organic matter (POM) independently from each other, which extended BC lifetime and BC impact. The GISS model simulated different concentration fields for natural aerosol (dust and sea-salt) in the two simulations (B and PRE) because heterogeneous concentrations changed e.g. the solubility of dust. This difference was not considered here as contributing to the "anthropogenic" RF term. Natural aerosols differ for the MPI_HAM model, where emissions of natural aerosol, in place of AeroCom suggestions, were implemented via an interactive source. The UIO-GCM model simply prescribed constant sea salt and dust fields for each month. The ULAQ model reports only clear sky forcing. The all-sky forcing was in ULAQ was assumed to be 30% of the clear-sky value (assuming 70% cloud cover and no aerosol forcing in cloud conditions). Most probably there are other differences between models, which we are not aware of. We feel that the methodological deviations documented here illustrate the unavoidable imperfection of a model intercomparison effort but that might help to guide future research.

3 Results

3.1 Sulphate aerosols

Model results for anthropogenic sulphate load, aerosol optical depth (AOD) and its fraction with respect to total sulphate are summarized in Table 2. Also listed in this table are model predictions for the sulphate RF and associated forcing efficiencies, forcing with respect to sulphate load and AOD, respectively. Results of AeroCom models are found in the lower part of the table and they are compared to recently published values,

provided in the upper part of the table. Average and standard deviation for the two groups of model results are placed at the bottom of the table to illustrate how much the coordinated AeroCom effort differs from model results found in the published literature.

Both groups of model results agree that sulphate exerts a negative RF, cooling the Earth-Atmosphere-System. Both sulphate burdens and optical depths are 25% smaller for the AeroCom models. Correspondingly, the mean of the RF estimate from the AeroCom models ($-0.35\,Wm^{-2}$) is 25% smaller than those published recently ($-0.46\,Wm^{-2}$). The revised and regionally shifted SO_2 emissions (less in Europe, more in Asia) used in AeroCom can explain this reduction. The mean forcing efficiency with respect to sulphate load (NRFM) or AOD (NRF) from AeroCom is only slightly different from that of the other model results.

However, RF results from individual model results still vary substantially, resulting in a significant standard deviation (ca. 40% on average) for load, AOD and RF. This diversity is larger than the difference between the averages from the two model groups. The diversity of RF among AeroCom models is only slightly smaller than that of the other model group. From this we can conclude that the prescribed emissions in AeroCom do not produce a significantly larger agreement among models.

Table 2 reports several other diagnostics, which may explain RF diversity among AeroCom models. The relative standard deviation in load (39%) is in effect both due to the variation in efficiency with which emitted SO_2 is transformed to aerosol sulphate (24%) and to the variation in the life time of sulphate in the atmosphere (26%). The example of the LOA and LSCE simulations is interesting because very similar models are used, with an identical transport model (LMDzT) and almost identical chemical sulphate production scheme (except for dynamic oxidant levels in the LSCE-model). The difference between LOA and LSCE in chemical production must be due to the different dry deposition scheme of the precursor gas SO_2. Another particular case is the low fine mode sulphate production in GISS, which is due to a significant loss of SO_2 on mineral dust.

On top of the sulphate load variation (39%) the mass extinction coefficient varies by

another 29% and those factors together explains that the sulphate AOD varies by 44%. The anthropogenic fraction of the total sulphate AOD varies by 15%, despite identical natural and anthropogenic sulphur emissions. It indicates that there are important differences in the models on the individual process level of the sulphur cycle. It is also interesting that the forcing efficiency per kg mass (NRFM) varies with 21% less than that of the forcing efficiency per unit optical depth (NRF) with 35%. A refined sensitivity analysis of the impact of different factors on RF diversity, using the additional results in Table 2, is done in Sect. 3.5. Altogether the variation analysis shows that several factors are equally important (with equally little model understanding) to link anthropogenic sulphur emissions to RF.

3.2 Carbonaceous aerosols

The different chemical components that belong to the carbonaceous aerosol give rise to controversial splits of the total carbonaceous aerosol forcing. Biomass burning aerosols have been shown to be rather homogeneous in nature, internally mixed to a large extent and with lower light absorption coefficients than soot particles emitted from high temperature combustion processes. Organic matter from fossil fuel burning has been suggested to be partly separated from soot particles. Secondary organic aerosol may be formed from volatile organic compound emissions without soot being necessarily present. For an overview of problems to characterize carbonaceous aerosols see Kanakidou et al. (2005). The three source categories, biomass burning (BB), fossil fuel black carbon (FFBC) and fossil fuel particulate organic matter (FFPOM) evidently do not fit all problems in attributing carbonaceous aerosol RF. While some models report fossil fuel and biomass burning aerosol RF separately, others use emission inventories that are already combined. To add complexity, measurements for both concentration and emission profiles often refer to an absorbing carbon component, summarised for simplicity as black carbon (BC), and a bulk chemical component, total organic carbon (TOC). TOC is recalculated to particulate organic matter (POM) by empirical conversion factors accounting for non-carbon material present. Both the measurement basis

of TOC and the prevailing internally mixed particle nature suggest that the three source categories mentioned above should be treated as a total carbonaceous category, which we name hereafter (BCPOM).

The AeroCom model results are heterogeneous with respect to identifying carbonaceous aerosol categories, because the model structure with respect to the split of the carbonaceous aerosols is difficult to change for just one experiment. To make the results from the different models more comparable we chose to compute the missing values. This is done based on ratios established within those models having explicitly dealt with the split of the carbonaceous particles. These ratios are derived from global mean values as reported in Tables 3 and 4 and should not be seen as valid on a local level. The computations are detailed in the footnotes of Tables 3 and 4.

Carbonaceous aerosol life times, loads and optical properties are found in Table 3. This table also reports AeroCom group results together with recently published data for comparison. Table 3 also contains simulated anthropogenic absorption AOD values for black carbon. As for sulphate, the diversity in POM load and AOD is as large among AeroCom models as in the other group of model results. The variation in POM mass extinction coefficient is relatively important (40%) as compared to that of POM lifetime (24%). The anthropogenic fraction of POM varies little (8%) but its variation indicates significant differences in removal patterns among models, given that the emissions were prescribed. However, the anthropogenic fraction of POM-AOD varies less than that of sulphate because, in contrast, an additional process (chemical production) affects the fate of the natural and anthropogenic sulphur emissions. BC lifetime is smaller than that of POM for half of the AeroCom models (L-P). However, the mass absorption coefficient of BC also shows considerable variation. The optical properties of BC and POM are a source of considerable diversity among the AeroCom models.

The corresponding RF values and forcing efficiencies are found in Table 4. The total BCPOM RF is positive (warming the Earth-Atmosphere System) in both model groups. As for sulphate, the RF suggested by the AeroCom models is slightly less important than that by non-AeroCom models (+0.14 instead of +0.26 Wm^{-2}). This is consistent

with smaller loads of both BC and POM in the AeroCom simulations, which can partly be explained by using prescribed biomass burning emission for the year 2000, which were relatively small compared to the average over the last decade (van der Werf et al., 2003).

The BCPOM RF estimates, and all other categories of carbonaceous aerosol RF, vary considerably. In light of the large differences for aerosol absorption among AeroCom models this is not completely surprising. Aerosol absorption makes RF calculations dependent on environmental factors, resulting in a less negative (or more positive) RF, especially when placed over highly reflective surfaces (e.g. snow or low clouds). In that context also spatial differences in burden distributions contribute (Fig. 1). Several models transport considerable amounts of BC towards the polar regions, while others efficiently remove BC close to emission sources (e.g. MPI-HAM and UIO_CTM). The diagnostics of long range transport is probably a good indicator of black carbon remaining at high altitudes, which in itself is a result of a less efficient washout process or an efficient vertical transport process parameterisation and differences in the treatment of black carbon ageing. An evaluation of the BC fields with measurement is beyond the scope of this paper, and will be performed in future work for the AeroCom results.

A word of caution is needed before the individual source categories of carbonaceous aerosol RF are discussed: Since gaps in the submitted model results were filled by recomputed values, the different estimates by source category (total BCPOM; total BC; total POM; fossil fuel BC: FFBC; fossil fuel POM: FFPOM and biomass burning: BB) are not completely independent of each other. There is general agreement between AeroCom and non-AeroCom models that the POM-RF is negative and that BC-RF is positive – resulting overall in a slightly positive combined BCPOM RF (on an annual global basis). Comparisons between forcings associated to biomass burning and fossil fuel burning suggest a more positive (or less negative) fossil fuel RF, which is consistent with higher BC/POM ratios for fossil fuel emissions.

The inspection of the consistency of the BCPOM-RF with the split into either BC-RF+POM-RF or into FFBC-RF+FFPOM-RF+BB-RF reveals that the total carbona-

ceous aerosol RF is not always a linear combination of the two sorts of splits. This is partly due to the method used for filling gaps, where ratios established in other models are used. Secondly it expresses the difficulty in ascribing a RF to individual carbonaceous aerosol source categories. The internal aerosol mixing and associated changes in forcing efficiency of especially black carbon but also POM is responsible for non-linear effects. The MPI_HAM model results serve as a good example in that here only the RF for total aerosol, sulphate and fossil fuel aerosol were available. BCPOM-RF must correspond to the difference between the total aerosol and sulphate RF. A relatively high positive BCPOM forcing then implies relatively large negative POM and positive BC contributions and the largest BB RF among all other models.

The diversity in component wise RF is largest for BB (160%) and BCPOM (79%). FF-BC forcing shows little variation (23%), while those of BC, POM and FFPOM vary around 60%. This is significantly larger than that of the sulphate RF. Also in absolute terms BB-RF shows more variation ($\pm 0.08\,\mathrm{Wm}^{-2}$) than the fossil fuel components (around $\pm 0.02\,\mathrm{Wm}^{-2}$). This is not only due to the MPI_HAM results and indicates altogether that the carbonaceous aerosol RF is responsible for an important part of the total RF diversity among models.

3.3 Total anthropogenic aerosol

All nine AeroCom models reported a component combined total aerosol RF based on the AeroCom emissions. Note again, that nitrate, ammonium and anthropogenic dust are not considered in AeroCom emissions. However, ammonium sulphate is implicitly assumed when deriving sulphate optical parameters. The RF values can be found in Table 5 along with global annual averages for aerosol load (or mass) and aerosol optical depth (AOD) and further diagnostics of the aerosol RF. The anthropogenic AOD fraction (of only 26% ±11% globally) leads to a negative all-sky RF of $-0.18\,\mathrm{Wm}^{-2}$ and a cooling of the Earth-Atmosphere-System, that is an order of magnitude smaller than the warming attributed to the anthropogenic enhancement of green-house gas concentrations. An overall warming by aerosol is unlikely, in the light of a low standard

deviation of ±0.16 Wm^{-2}. The non-AeroCom models show a similar RF of –0.23 Wm^{-2}.

The relatively small cooling due to the direct aerosol RF is the result of warming of the BC containing components and opposite cooling by POM and sulphate, as illustrated in Fig. 2. An explanation for the relatively small standard deviation of the total aerosol RF is that the magnitude of negative (POM) and positive (BC) forcing is correlated. Their RF is correlated, because the residence times of the carbonaceous aerosol components in a given model are already connected. The correlation coefficient between BC and POM residence times from nine AeroCom models is 0.92.

Figure 3 shows the zonal distribution of the total aerosol RF in the nine AeroCom models. Most of the (negative) RF is located between 20 and 60° N and forcing differences are largest, especially at northern mid-latitudes. The highest positive forcings in the northern regions by the GISS and the UIO_GCM models coincide with their relatively high BC loads there. Among all AeroCom models only SPRINTARS suggests a very weak positive forcing, which is most likely caused by its external mixing assumptions for BC and POM. Another SPRINTARS simulation (model C) with an even higher BC load (using non-AeroCom emissions; model G vs S in Table 3) but with a combined treatment of BC and POM results in a less negative forcing (Takemura et al., 2005).

The diversity of the RF among AeroCom models is as large as 89%. This is considerably larger than the diversity in load (24%), AOD (37%) and clear-sky forcing efficiency (45%). The reasons for the differences in forcing among the AeroCom models are the subject of discussion in the following sections. Based on the additional output provided by the AeroCom models, individual steps from emissions to forcing can be diagnosed.

The AeroCom diagnostics include two more parameters that concern changes of the radiation balance due to aerosol present in the atmosphere: "Atmospheric forcing" which accounts for solar absorption of incoming radiation in the atmospheric column – and "surface forcing" which reflects the incoming solar radiation at surface level, which is counterbalanced by other heat fluxes at surface level and is thus important for the hydrological cycle but which is not a good indicator of climate warming. The surface forcing equals the ToA-RF minus the atmospheric forcing. These are rarely reported in

other publications and shall be mentioned here, because they constitute an important element for the regional climate impact of the aerosol. The solar all-sky atmospheric forcing attains a global average of +0.85 Wm^{-2} and consequently the solar surface forcing is at –1.03 Wm^{-2}. The atmospheric forcing is considerably larger than the ToA-RF for all models. The absolute value of the diversity for the atmospheric forcing is comparable to that of RF. The relative standard deviation is only 20%. An inspection of the individual model values of RF and atmospheric forcing reveals that the two parameters are not correlated. Since atmospheric forcing should reflect absorption of shortwave radiation we have also tested correlation with the three major components. The highest correlation coefficient is found for BC-RF (r=0.46; without LOA r=0.71), while correlation with POM-RF (r=0.36) and SO4-RF (r=0.14) is absent. Measurements of the atmospheric forcing can thus be helpful to better understand the carbonaceous RF component.

3.4 Analysis of all-sky, clear-sky and cloud-sky forcing differences

The all-sky solar RF, which was discussed in the previous section, is in addition to parameters that influence clear-sky forcing also modulated by clouds. The clear-sky aerosol RF is influenced by aerosol properties (mainly amount and absorption), by the solar surface albedo and the distribution of water vapor. The presence of cloud changes the radiation field dramatically and can change the sign of aerosol RF. All-sky RF is consequently not just a cloud cover area-weighted clear-sky RF. Therefore we compare here the simulated annual global fields for all-sky (RF) and clear-sky ToA forcing (RF_{cs}) and cloud-sky ToA forcing (RF_{cl}) from the AeroCom simulations as summarized in Table 5. The cloud-sky forcing was not reported by modelers and is recomputed here based on global annual fields of RF, RF_{cs} and individual model derived information on cloud cover (C):

$$RF_{cl} = RF/C - (1 - C)/C^{*}RF_{cs}. \quad (1)$$

Clear-sky RF fields of most of the different AeroCom models in Fig. 4 display similar patterns. Negative forcings are predicted above industrialized zones of the Northern Hemisphere and over tropical biomass burning regions. Positive, or less negative, forcings are simulated over bright desert surfaces and over snow-cover. Larger differences among models over desert regions can be traced back to desert solar albedo assumptions not shown here. Positive forcings over ocean, as simulated only by the ULAQ model, can only be explained by strong aerosol absorption. The diversity of clear sky-forcing (47%) in Table 5 is found to be smaller than that of the all-sky RF (89%), which reflects better understanding of clear-sky radiative effects.

All-sky (aerosol) annual RF fields of the different AeroCom models in Fig. 5 indicate that the all-sky aerosol RF is almost everywhere less negative than clear-sky forcing (Fig. 4). Under all-sky conditions, the clear-sky forcing values apply only to cloud-free regions (ca. 30%), while in conjunction with clouds, aerosol (solar) RF is modulated depending among other parameters on the relative altitude between aerosol and clouds. If clouds are optically thick, solar radiation is reflected to a large part back to space, before it can interact with aerosol below the cloud. RF forcing by aerosol can then be ignored. If aerosol is above clouds, however, the high solar reflectivity of clouds will cause a warming, as observed over surfaces with large solar albedos (e.g. desert, snow). Now, eventually absorbing, aerosol reduces solar reflection to space, which translates into a positive ToA forcing (or warming).

We find that the cloud-sky aerosol ToA forcing is a useful diagnostic tool. Cloud-sky annual ToA forcing fields of the different AeroCom models in Fig. 6 display characteristic spatial features, which differ from model to model, and can be linked to physical explanations as found below. The diversity of cloud-sky forcing attains 50% just as much as that of the clear sky forcing (see Table 5). Global annual averages of RF, RF_{cs} and RF_{cl} are put together in Fig. 6. Globally averaged cloud-sky forcings vary between +0.34 and –0.16 Wm^{-2} and for almost all models deviate significantly from zero. Since under all-sky conditions cloud-cover is more likely than clear-sky, small differences of cloud-sky ToA forcing are an important explanation for the all-sky ToA forcing diversity

among the AeroCom models.

Why are models showing positive and negative cloud-sky forcings? An interesting comparison can be made for the LOA and the LSCE model. While the underlying GCM and thus meteorology and transport and emissions are the same, the aerosol dynamics, removal, optical properties and forcing calculations are not. The absolute difference in cloud cover is a result of different diagnostics provided to the AeroCom database. The relative cloud cover distribution is very much alike. We diagnose a negative cloud forcing for LOA and a slightly positive one for LSCE. Clear sky forcing in the LSCE is 20% more negative. Figure 5 shows similar positive forcing in LOA and LSCE in regions where continental pollution plumes reach out in the ocean area and in particular west of North and South Africa, west of North and South America, in the southern Indian ocean, east of Argentina and east of Japan. We can safely assume that absorbing anthropogenic aerosols above marine stratocumulus clouds are responsible for such positive cloud-sky forcing. The global average becomes negative for LOA because important negative cloud forcing contributions are diagnosed for North America, Europe and South East Asia. LOA also shows more negative sulphate forcing than LSCE. “Cloud forcing” of sulphate seems to impact the LOA results differently than that of LSCE.

Looking at all models we find that the three models with the largest negative aerosol all-sky RF also have negative cloud-sky forcings (UIO_CTM, UMI, LOA). Models with low BC loads (UIO_CTM, UMI) even fail to show positive all-sky forcing in any region. Elevated biomass burning aerosol seems to be responsible for positive cloud-sky forcing over the Atlantic off South Africa. UIO_CTM simulates such positive cloud-sky forcing only in the North American and South East Asian polluted areas. While UIO_CTM has a negative cloud sky RF for the annual mean the cloud-sky RF in the biomass burning season (July–September) is positive.

Positive cloud-sky forcings are responsible for the less negative all-sky forcing in LSCE, MPI_HAM, GISS and SPRINTARS. Note that the model with the largest cloud-sky forcing (SPRINTARS) also simulates the second largest BC loads. MPI_HAM

shows similar cloud-sky forcing over the ocean as LOA and LSCE, but simulates important positive contributions also over industrialised mid-latitude regions and above desert areas. This indicates a higher sensitivity of the RF to the albedo – either from bright desert surfaces or clouds. The GISS model despite having one of the lowest sulphate loads is characterised by negative all-sky forcing and positive cloud-sky forcing in the northern hemisphere and especially South East Asia and over the Pacific. Not all necessary diagnostics are available to understand the low all-sky forcings for the UIO_GCM and ULAQ models.

3.5 Sensitivity analysis of major factors linking emission and forcing

Having used identical emissions and analysed meteorology for the same year offers the chance to analyse the different steps from emission to forcing with small interference from large spatial differences in emission and aerosol fields. Few major factors are investigated here for their impact on resulting aerosol forcing diversity among AeroCom models. A simplified diagnostic model equation illustrates that the RF is a product of emission flux E, residence time (or life-time) (t), mass extinction efficiency (mass to AOD conversion) *mec* and the radiative forcing efficiency (NRF) with respect to AOD: RF=E**t***mec**NRF. Since the emissions E are equal, any variability of the three remaining factors (t, *mec*, and NRF) influences the simulated forcing. While this is valid for POM, factors of relevance were chosen differently for sulphate, BC and total aerosol. For the total aerosol we introduce the forcing efficiency for clear-sky RF and the ratio of all-sky RF over clear-sky RF as factors. BC RF is related to absorption AOD and a forcing efficiency per unit absorption AOD. Sulphate forcing depends also on the chemical production of aerosol sulphate.

Data from Tables 2, 3, 4 and 5 provide individual residence time, mass extinction coefficient and forcing efficiencies for sulphate, BC and POM and total aerosol. Then for each model n, factor x and species i the hypothetical $RF_{x,n,i}$ (for the case that only the factor x was a source of variability) is defined by $RF_{x,n,i}=x_n/\langle x\rangle * RF_i$, where x_n is the factor value for model n, <x> is the AeroCom mean for the factor and RF_i is the

mean AeroCom forcing for the aerosol species i.

All $RF_{x,n,i}$ are presented for each model and factor in Fig. 8 separately for the four species: sulphate, BB, POM and total aerosol. In addition, the original model derived RF values are shown in the last column. Model specific lines connect estimated $RF_{x,n,i}$ mainly for readability purposes. Cross-overs indicate compensating effects, which reduce model diversity for the "final" aerosol RF estimate.

The sensitivity for the total anthropogenic forcing in Fig. 8a shows that mainly the clear-sky forcing efficiency and the all-sky forcing calculation themselves are responsible for the diversity among the AeroCom models. However, it is probably not so much the radiative transfer calculation method, but differences in composition and most of all the representation of clouds that contribute to the diversity. In comparison, residence time and mass extinction efficiency introduce a relatively small diversity on total RF estimates. Numerous cross-overs indicate that each model has its own way of translating emission into forcing.

The sensitivity of BC forcing in Fig. 8b is discussed as a function of the aerosol absorption coefficient. The absorption coefficient based on the global values of absorption and load in Table 3 ranges from ∼4.5 (UMI and LSCE) up to ∼10 (SPRINTARS and UIO_GCM). In contrast to the sensitivity of the total aerosol RF, now BC residence time and BC absorption efficiency cause significant scatter in BC-RF. However, the forcing efficiency remains the major source of diversity. Inspecting the cross-overs of the modeled pathway from emission to forcing seems to indicate more confusion than for the total aerosol, although MPI-HAM diversity should be considered with caution. MPI_HAM simulations have not been performed for BC and POM separately and the uncertainties from retroactive split into BC and POM, resulting in values for Table 3, are largely responsible for erroneous mass extinction efficiencies.

The sensitivity analysis for POM-RF and sulphate-RF are presented in Figs. 8c and d, respectively. The two constituents are treated considerably differently in the AeroCom models. Sulphate residence times together with chemical production – in contrast to POM residence times – constitute a major source of diversity, because forma-

tion of sulphate involves additional processes, such as SO_2 deposition and chemical production in gas and cloud phase. Interestingly small sulphate production rates (or slow removal) are compensated considerably by high aerosol extinction coefficients for SPRINTARS, ULAQ, and UIO_CTM, and vice versa for LOA, LSCE, MPIHAM and partly GISS. Since hygroscopic growth is a major factor in enhancing sulphate aerosol extinction one might speculate if larger residence times result from sulphate transported into dry upper air tropospheric layers. This would coincide with little hygroscopic growth and thus would diminish the global extinction coefficient. Inspection of the AeroCom database shows that indeed LOA, LSCE and UMI have roughly four times as much sulphate burden located in the upper troposphere (>5 km) than models like SPRINTARS and UIO_CTM. POM residence times and extinction coefficients are minor sources of variation. With the exception of MPIHAM (see comment above) and SPRINTARS the variation in POM mass extinction coefficient is even negligible. A plausible hypothesis is that the models applied the same size distribution as suggested by the AeroCom emission dataset description and that little humidity growth is assumed for the organic particle fraction. Different forcing efficiencies for sulphate further seem to complicate the pathway towards forcing. Models with relatively high forcing efficiencies based on sulphate optical thickness are MPI_HAM (internal mixture?), GISS (despite relatively large size?) and UMI. The reason for this is not clear. Altogether we have to stress that among the three factors influencing the sulphur forcing estimate, none can be called the single major cause of diversity. For POM we find that the forcing efficiency gives rise to even larger diversity than found in the original forcing estimates in the model output. Note again, that the MPI-HAM results should be viewed with caution due to the retroactive source split when calculating component AOD values, which lead to unrealistic high forcing efficiencies for POM. Due to the lack of diagnostics we cannot verify here all the assumptions made for the POM forcing efficiencies. Internal and external mixing assumptions and absorption properties of the POM may not be as clearly split from the BC as would be needed to clearly understand the diversity in POM forcing efficiency. Aerosol water was unfortunately not diagnosed in the AeroCom B and PRE

experiment but would also be a good candidate for further studies.

4 Summary and conclusions

As a summary annual fields averaged from all regridded AeroCom model results are presented in Fig. 9 for anthropogenic aerosol optical depth, the associated RF, the local standard deviation of RF from the nine AeroCom models, solar atmospheric forcing and surface forcing as well as the clear-sky RF.

Anthropogenic aerosol optical depth shows distinct maxima in industrialised regions and above tropical biomass burning regions (Fig. 9a). The prevailing location of the anthropogenic aerosol is over continents. On average anthropogenic aerosol optical depth makes up only 26% of the total aerosol optical thickness. These two characteristics keep any comparison with satellite derived aerosol effects a challenging task, since the satellite observations are more reliable over the ocean. Furthermore Fig. 9e shows that the more readily observable clear-sky forcing is dominantly linked to high anthropogenic AOD over the continents.

The aerosol RF attains $-0.18\,Wm^{-2}$, suggesting a limited impact on climate from the presence of anthropogenic aerosol in the atmosphere. General cooling over the industrial regions of the northern hemisphere is partly offset by significant warming over desert regions in the sub-tropics and when biomass burning aerosol is present over oceanic low stratocumulus regions (Fig. 9a). A regional analysis of the diversity among models can be found in Fig. 9c. The local standard deviation of RF, based on the local annual averages of the nine AeroCom models, suggests that resolving the differences between the models should involve dedicated studies in four regions: South East Asia, African biomass burning areas, the European plume reaching out over the Eurasian continental area and the plume from Eastern North America going to the Atlantic. The local model diversity computed as standard deviation can reach $3\,Wm^{-2}$ in certain regions. This is an order of magnitude above the average RF. The large standard deviations for RF occur whenever models cannot agree on the sign of

the cloud-sky forcing. The average local standard deviation, provided at $\pm 0.27\,Wm^{-2}$, is larger than the standard deviation based on annual global averages of $\pm 0.16\,Wm^{-2}$ as presented in Table 5. This indicates that there is significant spatial variability in model diversity.

The solar atmospheric aerosol forcing, characterizing solar absorption by aerosol, displays local maxima over tropical biomass burning regions and over South East Asia, which can be as large as $+5\,Wm^{-2}$ on an annual basis (Fig. 9d). The local impact of the atmospheric aerosol forcing for changes in the surface energy budget can be deduced from Figure 9f. The map of surface forcing also illustrates that this aerosol effect is localised at different places than that of RF. Given the correlation of BC-RF and atmospheric forcing we suggest that places of large atmospheric forcing and larger corresponding surface forcing are preferred locations for a validation of the absorbing component in the models, and for field experiments.

Our sensitivity studies show that model diversity for residence time and calculated optical properties contribute significantly at times to simulated RF. More model data analysis needs to be done to understand the differences. The largest aerosol RF uncertainties are introduced when the modulating effect of clouds needs to be considered in all-sky simulations. A proper representation of cloud fields and the correct relative altitude placement between aerosol and clouds are needed.

To make advances on source attribution, experiments are needed that can identify more unambiguously the contributions of absorbing aerosols from specific source categories. The split in POM and BC from fossil fuel and biomass burning proves to be difficult, especially if model experiments are missing to separate these. If the overall effect of carbonaceous aerosols were known, then the opposing effects of absorbing BC and reflecting POM compounds would be better constrained. The sensitivity of the cloud-sky forcing to absorbing aerosol components adds motivation to focus on carbonaceous aerosols.

In conclusion, for the first time, a suite of global models with complex component aerosol modules has been employed and initialized with identical emissions in terms of

component, amount and size and meteorological fields for the same year. Based on the combination of simulations with nine different models a new estimate of aerosol direct radiative ToA forcing (without nitrate and dust) has been determined at $-0.2\,Wm^{-2}$ with an associated standard deviation of $\pm 0.2\,Wm^{-2}$. This suggests that the direct aerosol effect is small and negative (despite the potential for warming by absorbing aerosols especially over bright surfaces). This suggests that on a global annual basis the direct aerosol ToA forcing is opposite in sign and one order smaller than the impact attributed to anthropogenic greenhouse gases. However, local warming by greenhouse gases is easily compensated, especially over industrial regions of the northern hemisphere, in particular Southeast Asia, and over tropical regions during biomass burning seasons. On the other hand increased warming can be expected over regions with high solar surface albedo (e.g. desert and snow-covered terrain) and when tropical region biomass burning aerosol is advected over low clouds. The overall spread of the models with respect to the different forcing components, both globally and locally, is considerable. Furthermore the harmonised AeroCom emissions did not reduce model diversity The estimated RF diversity derived from the AeroCom simulations can be regarded as a minimum estimate for uncertainty in aerosol RF.

Acknowledgements. This work was among others supported by the European Project PHOENICS (Particles of Human Origin Extinguishing "natural" solar radiation In Climate Systems) under grant EVK2-CT-2001-00098. The authors would like to thank the Laboratoire des Sciences du Climat et de l'Environnement/IPSL, Gif-sur-Yvette, France, and the Max-Planck-Institut für Meteorologie, Hamburg, Germany for support in hosting the AeroCom database.

References

Adams, P. J., Seinfeld, J. H., Koch, D., Mickley, L., and Jacob, D.: General circulation model assessment of direct radiative forcing by the sulfate-nitrate-ammonium-water inorganic aerosol system, J. Geophys. Res.-Atmos., 106(D1), 1097–1111, 2001.

Anderson, T. L., Charlson, R. J., Schwartz, S. E., Knutti, R., Boucher, O., Rodhe, H., and

Heintzenberg, J.: Climate forcing by aerosols – a hazy picture, Science, 300(5622), 1103–1104, 2003.

Bellouin, N., Boucher, O., Haywood, J., and Reddy, M. S.: Global estimate of aerosol direct radiative forcing from satellite measurements, Nature, 438(7071), 1138–1141, 2005.

Berglen, T. F., Berntsen, T. K., Isaksen, I. S. A., and Sundet, J. K.: A global model of the coupled sulfur/oxidant chemistry in the troposphere: The sulfur cycle, J. Geophys. Res., 109, doi:10.1029/2003JD003948, 2004.

Boucher, O. and Pham, M.: History of sulfate aerosol radiative forcings, Geophys. Res. Lett., 29(9), 22–25, 2002.

Charlson, R. J., Schwartz, S. E., Hales, J. M., Cess, R. D., Coakley, J. A., Hansen, J. E., and Hofmann, D. J.: Climate forcing by anthropogenic aerosols, Science, 255, 423–430, 1992.

Chung, S. H. and Seinfeld, J. H.: Global distribution and climate forcing of carbonaceous aerosols, J. Geophys. Res., 107(D19), 4407, doi:10.1029/2001JD001397, 2002.

Dentener, F., Kinne, S., Bond, T., Boucher, O., Cofala, J., Generoso, S., Ginoux, P., Gong, S., Hoelzemann, J., Ito, A., Marelli, L., Penner, J., Putaud, J.-P., Textor, C., Schulz, M., van der Werf, G., and Wilson, J.: Emissions of primary aerosol and precursor gases in the years 2000 and 1750, prescribed data-sets for AeroCom, Atmos. Chem. Phys. Discuss., 6, 2703–2763, 2006.

Ghan, S., Laulainen, N., Easter, R., Wagener, R., Nemesure, S., Chapman, E., Zhang, Y., and Leung, R.: Evaluation of aerosol direct radiative forcing in MIRAGE, J. Geophys. Res., 106, 5295–5316, 2001.

Ghan, S. J., Easter, R. C., Chapman, E. G., Abdul-Razzak, H., Zhang, Y., Leung, L. R., Laulainen, N. S., Saylor, R. D., and Zaveri, R. A.: A physically based estimate of radiative forcing by anthropogenic sulfate aerosol, J. Geophys. Res.-Atmos., 106(D6), 5279–5293, 2001.

Hansen, J., Sato, M., Ruedy, R., Nazarenko, L., Lacis, A., Schmidt, G. A., Russell, G., Aleinov, I., Bauer, M., Bauer, S., Bell, N., Cairns, B., Canuto, V., Chandler, M., Cheng, Y., Del Genio, A., Faluvegi, G., Fleming, E., Friend, A., Hall, T., Jackman, C., Kelley, M., Kiang, N., Koch, D., Lean, J., Lerner, J., Lo, K., Menon, S., Miller, R., Minnis, P., Novakov, T., Oinas, V., Perlwitz, Ja., Perlwitz, Ju., Rind, D., Romanou, A., Shindell, D., Stone, P., Sun, S., Tausnev, N., Thresher, D., Wielicki, B., Wong, T., Yao, M., and Zhang, S.: Efficacy of Climate Forcings, J. Geophys. Res., 110, D18104, doi:10.1029/2005JD0057762005.

Iversen, T. and Seland, O.: A scheme for process-tagged SO4 and BC aerosols in NCAR

CCM3: Validation and sensitivity to cloud processes, J. Geophys. Res., 107(D24), 4751, doi:10.1029/2001JD000885, 2002.

Jacobson, M. Z.: Global direct radiative forcing due to multicomponent anthropogenic and natural aerosols, J. Geophys. Res.-Atmos., 106(D2), 1551–1568, 2001.

Kiehl, J. T., Schneider, T. L., Rasch, P. J., Barth, M. C., and Wong, J. : Radiative forcing due to sulfate aerosols from simulations with the National Center for Atmospheric Research Community Climate Model, Version 3, J. Geophys. Res.-Atmos., 105(D1), 1441–1457, 2000.

Kinne, S., Schulz, M., Textor, C., Guibert, S., Balkanski, Y., Bauer, S. E., Berntsen, T., Berglen, T. F., Boucher, O., Chin, M., Collins, W., Dentener, F., Diehl, T., Easter, R., Feichter, J., Fillmore, D., Ghan, S., Ginoux, P., Gong, S., Grini, A., Hendricks, J., Herzog, M., Horowitz, L., Isaksen, I., Iversen, T., Kirkevåg, A., Kloster, S., Koch, D., Kristjansson, J. E., Krol, M., Lauer, A., Lamarque, J. F., Lesins, G., Liu, X., Lohmann, U., Montanaro, V., Myhre, G., Penner, J., Pitari, G., Reddy, S., Seland, O., Stier, P., Takemura, T., and Tie, X.: An AeroCom initial assessment optical properties in aerosol component modules of global models, Atmos. Chem. Phys., 6, 1815–1834, 2006.

Kirkevag, A. and Iversen, T.: Global direct radiative forcing by process-parameterized aerosol optical properties, J. Geophys. Res.-Atmos., 107(D20), 4433, doi:10.1029/2001JD000886, 2002.

Koch, D.: Transport and direct radiative forcing of carbonaceous and sulfate aerosols in the GISS GCM, J. Geophys. Res.-Atmos., 106(D17), 20 311–20 332, 2001.

Koch, D., Schmidt, G. A., and Field, C.: Sulfur, sea salt and radionuclide aerosols in GISS, ModelE, J. Geophys. Res., 111, D06206, doi:10.1029/2004JD005550, 2006.

Liao, H. and Seinfeld, J.: Global impacts of gas-phase chemistry-aerosol interactions on direct radiative forcing by anthropogenic aerosols and ozone, J. Geophys. Res., 110(D18), D18208, doi:10.1029/2005JD005907, 2005.

Liao, H., Seinfeld, J. H., Adams, P. J., and Mickley, L. J.: Global radiative forcing of coupled tropospheric ozone and aerosols in a unified general circulation model, J. Geophys. Res.-Atmos., 109(D16), D16207, doi:10.1029/2003JD004456, 2004.

Liepert, B. G., Feichter, J., Lohmann, U., and Roeckner,E. : Can aerosols spin down the water cycle in a warmer and moister world?, Geophys. Res. Lett., 31(6), L06207, doi:10.1029/2003GL019060, 2004.

Liu, H. Q., Pinker, R. T., and Holben, B. N.: A global view of aerosols from merged transport models, satellite, and ground observations, J. Geophys. Res.-Atmos., 110(D10), D10S15,

doi:10.1029/2004JD004695, 2005.
Liu, X. and Penner, J. E.: Effect of Mt. Pinatubo H2SO4/H2O aerosol on ice nucleation in the upper troposphere using a global chemistry and transport model (IMPACT), J. Geophys. Res., 107, 4141, doi:10.1029/2001JD000455, 2002.
Martin, S. T., Hung, H. M., Park, R. J., Jacob, D. J., Spurr, R. J. D., Chance, K. V., and Chin, M.: Effects of the physical state of tropospheric ammonium-sulfate-nitrate particles on global aerosol direct radiative forcing, Atmos. Chem. Phys., 4, 183–214, 2004.
Menon, S., Hansen, J., Nazarenko, L., and Luo, Y. F.: Climate effects of black carbon aerosols in China and India, Science, 297(5590), 2250–2253, 2002.
Ming, Y., Ramaswamy, V., Ginoux, P. A., and Horowitz, L. W.: Direct Radiative Forcing of Anthropogenic Organic Aerosol, J. Geophys. Res., 110, D20208, doi:10.1029/2004JD00553, 2005.
Myhre, G., Berntsen,, T. K., Haywood, J. M., Sundet, J. K., Holben, B. N., Johnsrud, M., and Stordal, F.: Modelling the solar radiative impact of aerosols from biomass burning during the Southern African Regional Science Initiative (SAFARI-2000) experiment, J. Geophys. Res., 108, 8501, doi:10.1029/2002JD002313, 2003.
Myhre, G., Stordal, F., Berglen, T. F., Sundet, J. K., and Isaksen, I. S. A.: Uncertainties in the radiative forcing due to sulfate aerosols, J. Atmos. Sci., 61(5), 485–498, 2004.
Pitari, G., Mancini, E., Rizi, V., and Shindell, D. T. : Impact of future climate and emissions changes on stratospheric aerosols and ozone, J. Atmos. Sci., 59, 414–440, 2002.
Ramaswamy, V., Boucher, O., Haigh, J. D., Hauglustaine, D. A., Haywood, J. M., Myhre, G., T. Nakajima, Shi, G. Y., and Solomon, S. : Radiative forcing of climate change, in: Climate Change 2001: The Scientific Basis, Contribution of Working Group I to the Third Assessment Report of the Intergovernmental Panel on Climate Change, edited by: Houghton, J. T., Ding, Y., Griggs, D. J., Noguer, M., van der Linden, P. J., Dai, X., Maskell, K., and Johnson, C. A., 349–416, Cambridge University Press, Cambridge, UK, 2001.
Reddy, M. S. and Boucher, O. : A study of the global cycle of carbonaceous aerosols in the LMDZT general circulation model, J. Geophys. Res., 109(D14), D14202, 2004.
Reddy, M. S., Boucher, O., Balkanski, Y., and Schulz, M.: Aerosol optical depths and direct radiative perturbations by species and source type, Geophys. Res. Lett., 32, L12803, doi:10.1029/2004GL021743, 2005a.
Reddy, M. S., Boucher, O., Bellouin, N., Schulz, M., Balkanski, Y., Dufresne, J. L., and Pham, M.: Estimates of global multicomponent aerosol optical depth and direct radiative perturba-

tion in the Laboratoire de Meteorologie Dynamique general circulation model, J. Geophys. Res.-Atmos., 110(D10), D10S16, doi:10.1029/2004JD004757, 2005b.
Stanhill, G. and Cohen, S.: Global dimming: a review of the evidence for a widespread and significant reduction in global radiation with discussion of its probable causes and possible agricultural consequences, Agric. Forest Meteorol., 107(4), 255–278, 2001.
Stier, P., Feichter, J., Kinne, S., Kloster, S., Vignati, E., Wilson, J., Ganzeveld, L., Tegen, I., Werner, M., Balkanski, Y., Schulz, M., Boucher, O., Minikin, A., and Petzold, A.: The aerosol-climate model ECHAM5-HAM, Atmos. Chem. Phys., 5, 1125–1156, 2005.
Takemura, T., Nakajima, T., Dubovik, O., Holben, B. N., and Kinne, S.: Single-scattering albedo and radiative forcing of various aerosol species with a global three-dimensional model, J. Climate, 15(4), 333–352, 2002.
Takemura, T., Nakajima, T., Nozawa, T., and Aoki, K.: Simulation of future aerosol distribution, radiative forcing, and long-range transport in East Asia, J. Meteorol. Soc. Japan, 79(6), 1139–1155, 2001.
Takemura, T., Nozawa, T., Emori, S., Nakajima, T. Y., and Nakajima, T.: Simulation of climate response to aerosol direct and indirect effects with aerosol transport-radiation model, J. Geophys. Res.-Atmos., 110, D02202, doi:10.1029/2004JD005029, 2005.
Textor, C., Schulz, M., Guibert, S., Kinne, S., Balkanski, Y., Bauer, S., Berntsen, T., Berglen, T., Boucher, O., Chin, M., Dentener, F., Diehl, T., Easter, R., Feichter, H., Fillmore, D., Ghan, S., Ginoux, P., Gong, S., Grini, A., Hendricks, J., Horowitz, L., Huang, P., Isaksen, I., Iversen, T., Kloster, S., Koch, D., Kirkevåg, A., Kristjansson, J. E., Krol, M., Lauer, A., Lamarque, J. F., Liu, X., Montanaro, V., Myhre, G., Penner, J., Pitari, G., Reddy,S., Seland, Ø., Stier, P., Takemura, T., and Tie, X.: Analysis and quantification of the diversities of aerosol life cycles within AeroCom, Atmos. Chem. Phys., 6, 1777–1813, 2006.
van der Werf, G. R., Randerson, J. T., Collatz, G. J., and Giglio, L.: Carbon emissions from fires in tropical and subtropical ecosystems, Global Change Biol., 9(4), 547–562, 2003.
Wang, C.: A modelling study on the climate impacts of black carbon aerosols, J. Geophys. Res.-Atmos., 109(D3), D03106, doi:10.1029/2003JD004084, 2004.

Table 1. Model names and corresponding models and version names, their resolution used here and selected principal publications associated to each model. See also Textor et al. (2006) for more complete descriptions of the models. "*" signifies a climatological model was run for a five year period. All other models are driven by analysed meteorological fields (nudged climate model or chemical transport model).

Model	Model type and version	Resolution	Levels	References
UMI	CTM IMPACT	2.5°×2°	30	(Liu et al., 2005; Liu and Penner, 2002)
UIO_CTM	CTM OsloCTM2	2.81°×2.81°	40	(Berglen et al., 2004; Myhre et al., 2003)
LOA	GCM LMDzT 3.3	3.75°×2.5°	19	(Reddy and Boucher, 2004; Reddy et al., 2005b)
LSCE	GCM LMDzT 3.3-INCA	3.75°×2.5°	19	(Textor et al., 2006)
MPI_HAM	GCM ECHAM5.2-HAM	1.8°×1.8°	31	(Stier et al., 2005)
GISS	GCM model E	5°×4°	20	(Koch, 2001; Koch et al., 2006)
UIO_GCM	GCM* CCM3.2	2.81°×2.81°	18	(Iversen and Seland, 2002; Kirkevag and Iversen, 2002)
SPRINTARS	GCM CCSR/NIES/FRCGC SPRINTARS 5.7b	1.1°×1.1°	20	(Takemura et al., 2002, 2005)
ULAQ	CTM* ULAQ	22.5°×10°	26	(Pitari et al., 2002)

Table 2. Sulphate aerosol forcing related global mean values, derived from recent publications (Models A-L) and from this studies AeroCom simulations, using identical emissions (Models M-U). All values refer to the anthropogenic perturbation of atmospheric sulphur. "CheProdSO_4/Emi-SO_2": Chemical production of aerosol sulphate over sulphur-emission; "Life time" derived from sulphate burden and chemical production; "MEC": mass extinction coefficient derived from load and sulphate aerosol optical depth ($\tau_{aer-so4}$); gτ_{aer} anthrop.": fraction of anthropogenic sulfate to total sulfate τ_{aer} of present day; "RF": shortwave radiative forcing; "NRFM": normalized RF by load; "NRF": normalized RF per unit g$\tau_{aer-so4}$.

No	Model	CheProdSO_4/ Emi-SO_2	Life time SO_4 [days]	Load [mg SO_4 m^{-2}]	MEC [m^2 g^{-1} SO_4]	τ_{aer}–SO_4	τ_{aer-} SO_4 anthrop. [%]	RF [Wm^{-2}]	NRFM [Wg^{-1}]	NRF [Wm^{-2} τ_{aer}^{-1}]	Reference
A	CCM3			2.23				–0.56	–251		(Kiehl et al., 2000)
B	GEOSCHEM			1.53		0.018		–0.33	–216	–18	(Martin et al., 2004)
C	GISS			3.30		0.022		–0.65	–206	–32	(Koch, 2001)
D	GISS			3.27				–0.96	–293		(Adams et al., 2001)
E	GISS			2.12				–0.57	–269		(Liao and Seinfeld, 2005)
F	SPRINTARS			1.55		0.015	72%	–0.21	–135	–8	(Takemura et al., 2005)
G	LMD			2.76				–0.42	–152		(Boucher and Pham, 2002)
H	LOA			3.03		0.030		–0.41	–135	–14	(Reddy et al., 2005a)
I	GATORG			4.29				–0.31	–72		(Jacobson, 2001)
J	PNNL			5.50		0.042		–0.44	–80	–10	(Ghan et al., 2001)
K	UIO_CTM			1.79		0.019		–0.37	–207	–19	(Myhre et al., 2004)
L	UIO-GCM			2.28				–0.29	–127		(Kirkevag and Iversen, 2002)
M	UMI	63%	4.8	2.64	7.8	0.020	58%	–0.58	–220	–28	This study
N	UIO_CTM	58%	3.3	1.70	11.0	0.019	57%	–0.35	–208	–19	This study
O	LOA	85%	4.8	3.64	9.6	0.035	64%	–0.49	–136	–14	This study
P	LSCE	70%	4.9	3.01	7.5	0.023	59%	–0.42	–138	–18	This study
Q	MPI_HAM	71%	3.9	2.47	6.3	0.016	60%	–0.46	–186	–29	This study
R	GISS	30%	5.1	1.34	4.4	0.006	41%	–0.19	–139	–31	This study
S	UIO_GCM	59%	3.3	1.72	6.8	0.012	59%	–0.25	–145	–21	This study
T	SPRINTARS	58%	2.3	1.19	10.8	0.013	59%	–0.16	–137	–13	This study
U	ULAQ	60%	3.0	1.62	12.1	0.020	42%	–0.22	–136	–11	This study
Average models A-L				2.80		0.024		–0.46	–176	–17	
Average models M-U		62%	3.9	2.15	8.5	0.018	55%	–0.35	–161	–20	This study
Stddev A-L			1.18		0.010		0.20	75	9		
Stddev M-U		15%	1.0	0.83	2.5	0.008	8%	0.15	34	7	This study
Stddev/Avg M-U		24%	26%	39%	29%	44%	15%	43%	21%	35%	

Table 3. Global mean values of load and optical properties of carbonaceous aerosol. All values correspond to the anthropogenic fraction. Life times are calculated from emission and load. POM: Particulate organic matter; BC: black carbon. MEC: mass extinction coefficient. Lines A-K: recently published model simulations; Lines L-T: Models used AeroCom emissions.

No	Model	Life time POM [days]	Load POM [mg m^{-2}]	MEC POM [m^{2}g^{-1}]	τ_{aer} POM	τ_{aer} POM anthrop. fraction	Life time BC [days]	Load BC [mg m^{-2}]	MABS BC [m^{2}g^{-1}]	$\tau_{aer-abs}$ BC [ ] *1000	Reference
A	SPRINTARS										(Takemura et al., 2001)
B	LOA		2.33		0.016			0.37			(Reddy et al., 2005a)
C	GISS		1.86		0.017			0.29			(Hansen and Mki. Sato, 2005)
D	GISS		1.86		0.015			0.29			(Koch, 2001)
E	GISS		2.39					0.39			(Chung and Seinfeld, 2002)
F	GISS		2.49					0.43			(Liao and Seinfeld, 2005)
G	SPRINTARS		2.67		0.029	82%		0.53			(Takemura et al., 2005)
H	GATORG							0.45			(Jacobson, 2001)
I	MOZGN		3.03		0.018						(Ming et al., 2006)
J	CCM							0.33			(Wang, 2004)
K	UIO-GCM							0.30			(Kirkevag and Iversen, 2002)
L	UMI	6.6	1.16	5.2	0.0060	53%	5.8	0.19	6.8	1.29	This study
M	UIO_CTM	6.4	1.12	5.2	0.0058	55%	5.5	0.19	7.2	1.34	This study
N	LOA	8.0	1.41	6.0	0.0085	52%	7.3	0.25	8.0	1.98	This study
O	LSCE	8.6	1.50	5.3	0.0079	46%	7.5	0.25	4.4	1.11	This study
P	MPI_HAM	6.1	1.06+	2.6	0.0028+	55%+	5.2	0.18+	9.0	1.58+	This study
Q	GISS	7.0	1.22	4.9	0.0060	51%	7.2	0.24	7.6	1.83&	This study
R	UIO_GCM	5.0	0.88	5.3	0.0046	59%	5.5	0.19	10.5	1.95	This study
S	SPRINTARS	10.5	1.84	10.8	0.0200	49%	10.6	0.37	9.8	3.50	This study
T	ULAQ	9.8	1.71	4.4	0.0075	58%	11.4	0.38	7.5	2.90	This study
Average A-K			2.38		0.019			0.38			
Average L-T		7.6	1.32	5.5	0.008	53%	7.3	0.25	7.9	1.94	This study
Stddev A-K			0.42		0.006			0.08			
Stddev L-T		1.8	0.32	2.2	0.005	4%	2.3	0.08	1.8	0.79	This study
Stddev/Avg L-T		24%	24%	40%	63%	8%	32%	32%	23%	41%	

+ MPI_HAM: Anthropogenic fraction derived from total POM and BC diagnostics: POM_{ant}=POM*0.55; BC_{ant}=BC*0.8

Table 4. Anthropogenic carbonaceous aerosol forcing. "NRF POM": normalized RF per unit gτ_{aer-} POM ; "NRF POM": normalized RF per absorption unit g$\tau_{aer-abs}$ BC ; BB=biomass burning sources included, FFBC=fossil fuel black carbon, FFPOM= fossil fuel particulate organic matter. Lines A-K: recently published/Lines L-T: Models used AeroCom emissions.

No	Model	NRF POM [Wm^{-2} τ_{aer}^{-1}]	NRF BC [Wm^{-2} $\tau_{aer-abs}^{-1}$]	RF BCPOM [Wm^{-2}]	RF POM [Wm^{-2}]	RF BC [Wm^{-2}]	RF FFPOM [Wm^{-2}]	RF FFBC [Wm^{-2}]	RF BB [W m^{-2}]	Reference
A	SPRINTARS			0.12	–0.24	0.36	–0.05	0.15	–0.01	(Takemura et al., 2001)
B	LOA			0.30	–0.25	0.55	–0.02	0.19	0.14	(Reddy et al., 2005a)
C	GISS			0.35	–0.26	0.61	–0.13	0.49	0.065	(Hansen and Mki. Sato, 2005)
D	GISS			0.05	–0.30	0.35	–0.08$^{\$}$	0.18$^{\$}$	–0.05$^{\$}$	(Koch, 2001)
E	GISS			0.32	–0.18	0.50	–0.05$^{\$}$	0.25$^{\$}$	0.12$^{\$}$	(Chung and Seinfeld, 2002)
F	GISS			0.30	–0.23	0.53	–0.06$^{\$}$	0.27$^{\$}$	0.09$^{\$}$	(Liao and Seinfeld, 2005)
G	SPRINTARS			0.15	–0.27	0.42	–0.07$^{\$}$	0.21$^{\$}$	0.01$^{\$}$	(Takemura et al., 2005)
H	GATORG			0.47	–0.06	0.53	–0.01$^{\$}$	0.27$^{\$}$	0.22$^{\$}$	(Jacobson, 2001)
I	MOZGN				–0.34					(Ming et al., 2006
J	CCM					0.34				(Wang, 2004)
K	UIO-GCM					0.19				(Kirkevag and Iversen, 2002)
L	UMI	–38	300	0.02	–0.23	0.25	–0.06$^{\$}$	0.12$^{\$}$	-0.01	This study
M	UIO_CTM	–3	24	0.02	–0.09$^{@}$	0.10$^{@}$	–0.04	0.11	-0.05	This study
N	LOA	–19	135	0.14$^{\#}$	–0.16$^{\#}$	0.27$^{\#}$	–0.04$^{\$}$	0.13$^{\$}$	0.05$^{\$}$	This study
O	LSCE	–21	274	0.13	–0.17	0.30	–0.04$^{\$}$	0.15$^{\$}$	0.02$^{\$}$	This study
P	MPI_HAM	–140	407	0.34$^{\#}$	–0.39$^{\#}$	0.64$^{\#}$	–0.05^{+}	0.16^{+}	0.23$^{\$}$	This study
Q	GISS	–23	120	0.08	–0.14	0.22	–0.03$^{\$}$	0.11$^{\$}$	0.01$^{\$}$	This study
R	UIO_GCM	–58	184	0.24	–0.06	0.36	–0.02$^{\$}$	0.18$^{\$}$	0.08$^{\$}$	This study
S	SPRINTARS	–5	91	0.22	–0.10	0.32	–0.01	0.13	0.06	This study
T	ULAQ	–9	55	0.10$^{\&}$	–0.07	0.16	–0.02$^{\$}$	0.08$^{\$}$	0.03$^{\$}$	This study
Average A-K				0.26	–0.24	0.44	–0.06	0.25	0.07	
Average L-T		–22	177	0.14	–0.16	0.29	–0.03	0.13	0.05	This study
Stddev A-K				0.14	0.08	0.13	0.04	0.11	0.09	
Stddev L-T		43	126	0.11	0.10	0.15	0.02	0.03	0.08	This study
Stddev/Avg L-T		195%	71%	79%	63%	52%	67%	23%	160%	

$ Models A–C are used to provide a split in sources derived from total POM and total BC; FFPOM=POM*0.25; FFBC=BC*.5; BB=(BCPOM)-(FFPOM+FFBC)

Models L,O,Q-T are used to provide a split in components: BCPOM=Total aerosol – SO4; POM=BCPOM*-1.15; BC=BCPOM*1.9

+ MPI_HAM fossil fuel carbonaceous forcing of –0.11 Wm^{-2}, POMant=POM*0.55; Bcant=BC*0.8

& ULAQ all sky values=clear-sky*0.3; GISS absorption coefficient assumed to equal that of AeroCom models (7.4 m^2 g^{-1})

@ Estimated using the fractions used in calculation of the optical properties

Table 5. AeroCom (models H-P) and recent other model estimates (A-G) simulation results of anthropogenic aerosol load, anthropogenic aerosol optical depth (τ_{aer}), its fraction of present day total aerosol optical depth (τ_{aerant}), a gross mass extinction coefficient (MEC) as well as cloud cover and clear-sky forcing efficiency per unit AOD. The all-sky total aerosol direct radiative forcing RF values are accompanied by the clear-sky and cloud-sky components together with their ratio. Solar surface forcing and solar atmospheric forcing are given for all-sky conditions.

No	Model	Load [mg m^{-2}]	τ_{aer}	τ_{aer} anthrop fraction	MEC [m^{2}g^{-1}]	Cloud cover	NRF clear-sky [Wm$^{-2}\tau_{maer}^{-1}$]	RF all-sky/ clear-sky	RF top clear sky [W m^{-2}]	RF top cloud-sky [W m^{-2}]	RF top] all-sky [W m^{-2}	surface forcing all-sky [W m^{-2}]	Atmos-pheric forcing all-sky [W m^{-2}]	Reference
											−0.39[&]	−1.98[&]	1.59[&]	
A	GISS	5.0				79%					+0.01[$]	−2.42[$]	2.43[$]	(Liao and Seinfeld, 2005)
B	LOA	6.0	0.049	34%		70%			−0.53		−0.09			(Reddy and Boucher, 2004)
C	SPRINTARS	4.8	0.044	50%		63%			−0.77		−0.06	−1.92	1.86	(Takemura et al., 2005)
D	UIO-GCM	2.7				57%					−0.11			(Kirkevag and Iversen, 2002)
E	GATORG								−0.89		−0.12			(Jacobson, 2001)
F	GISS	6.7	0.049								−0.23			(Hansen and Mki. Sato, 2005)
G	GISS	5.6	0.040								−0.63			(Koch, 2001)
H	UMI	4.0	0.028	25%	7.0	63%	−29	0.51	−0.80	-0.10	−0.41	−1.24	0.84	This study
I	UIO_CTM	3.0	0.026	19%	8.5	70%	-33	0.40	−0.85	-0.07	−0.34	−0.95	0.61	This study
J	LOA	5.3	0.046	28%	8.7	70%	−18	0.44	−0.80	-0.16	−0.35	−1.49	1.14	This study
K	LSCE	4.8	0.033	40%	6.9	62%	−29	0.30	−0.94	0.08	−0.28	−0.93	0.66	This study
L	MPI_HAM	4.3	0.042	30%	9.6	62%	−12	0.25	−0.50	0.14	−0.12	−1.07	0.95	This study
M	GISS	2.8	0.014	11%	5.0	57%	−21	0.36	-0.29	0.05	−0.11	−0.81	0.79	This study
N	UIO_GCM	2.8	0.017	11%	6.2	57%					−0.01	−0.84	0.84	This study
O	SPRINTARS	3.2	0.036	44%	11.1	62%	−10	−0.12	−0.35	0.34	+0.04	−0.91	0.96	This study
P	ULAQ	3.7	0.030	23%	8.1		-8	0.32	-0.25		−0.08			This study
Average A-G		5.1	0.046	42%					−0.73		−0.23	−1.95	1.73	
Average H-P		3.8	0.030	26%	7.9	63%	−20	0.31	−0.60	0.04	−0.18	−1.03	0.85	
Stddev A-G		1.4	0.004						0.18		0.21			
Stddev H-P		0.9	0.011	11%	1.7	5%	10	0.19	0.28	0.17	0.16	0.23	0.17	
Stddev/Avg H-P		24%	37%	42%	22%	8%	45%	61%	47%	50%	89%	22%	20%	

[&] External mixture
[$] Internal mixture

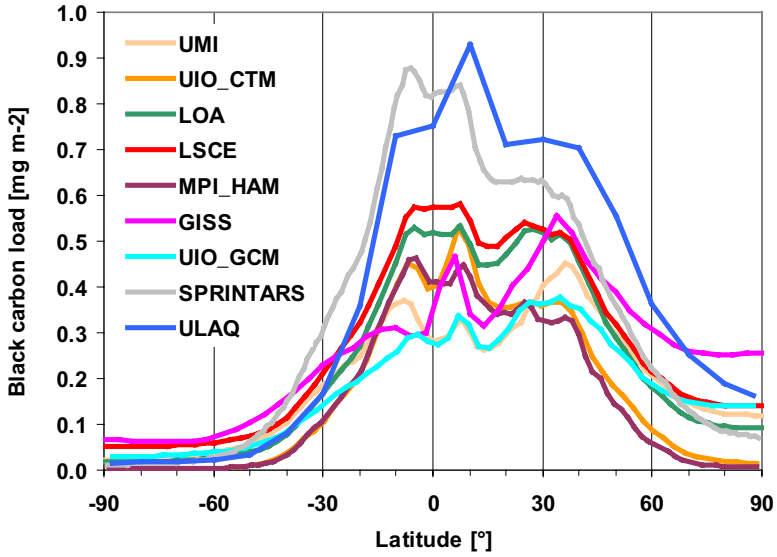

Fig. 1. Zonal distribution of the atmospheric load of black carbon for the AEROCOM B (present-day emissions) simulation.

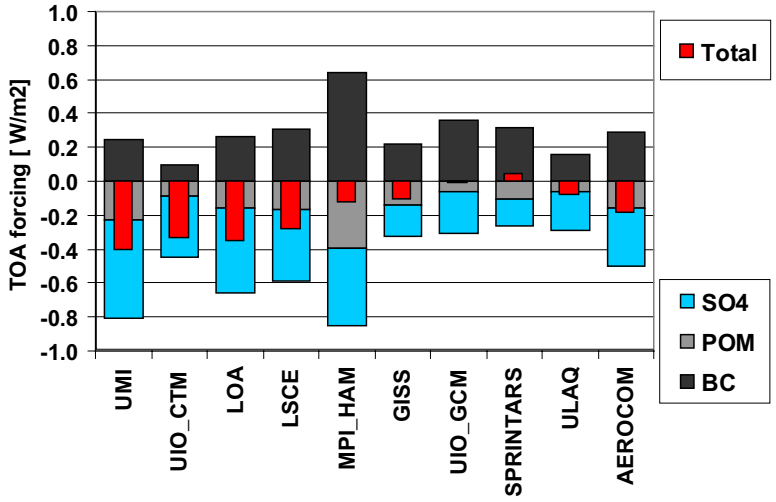

Fig. 2. Direct aerosol forcing for the three major anthropogenic aerosol components sulphate, black carbon and particulate organic matter in the AeroCom models. Shown on top in red is also the total direct aerosol forcing as diagnosed from a full aerosol run.

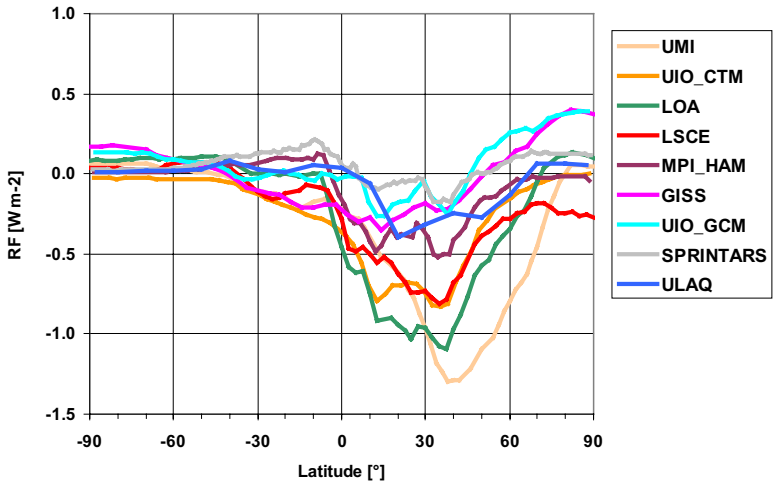

Fig. 3. Zonal distribution of the total direct aerosol forcing in all-sky conditions.

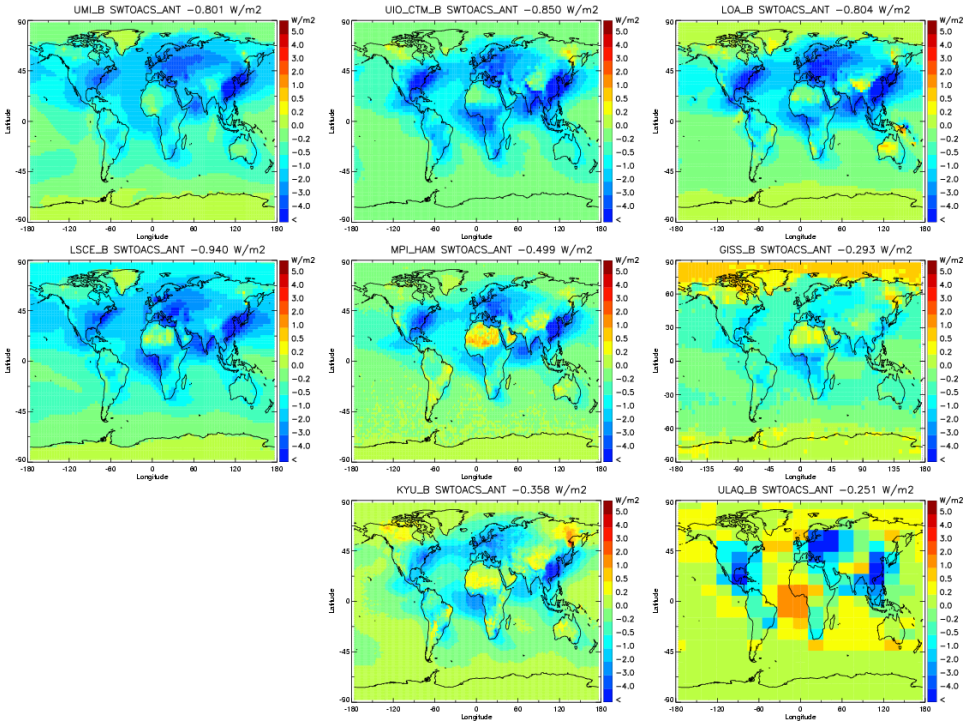

Fig. 4. Maps of the total direct aerosol forcing in clear-sky conditions in the AeroCom models. (note KYU=SPRINTARS model, will be replaced for next version).

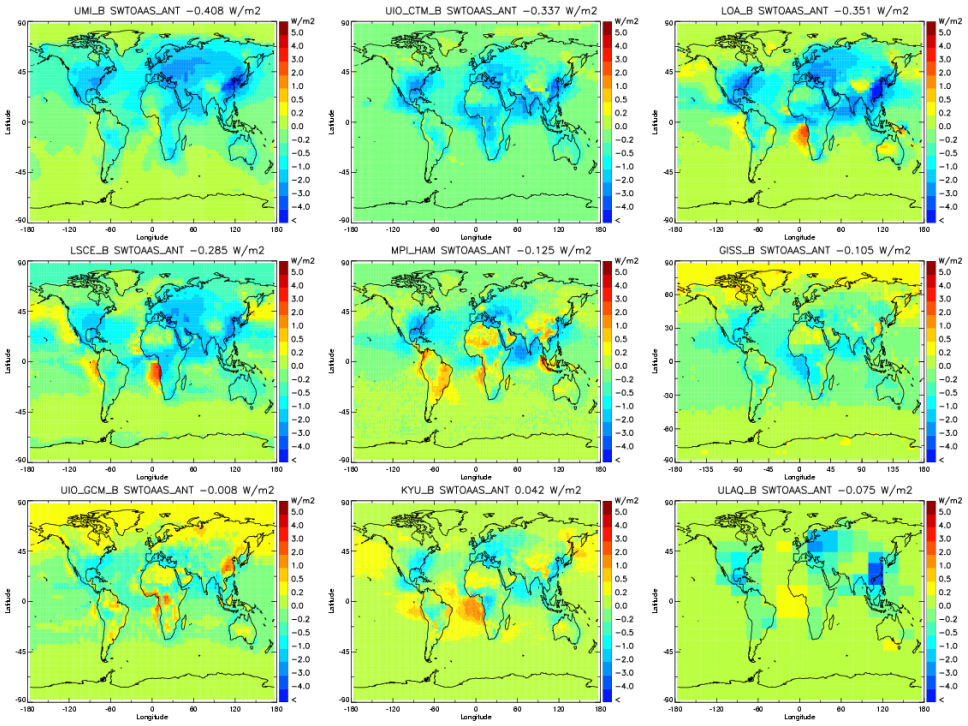

Fig. 5. Same as Fig. 4 but all-sky condition total direct aerosol forcing in the AeroCom models.

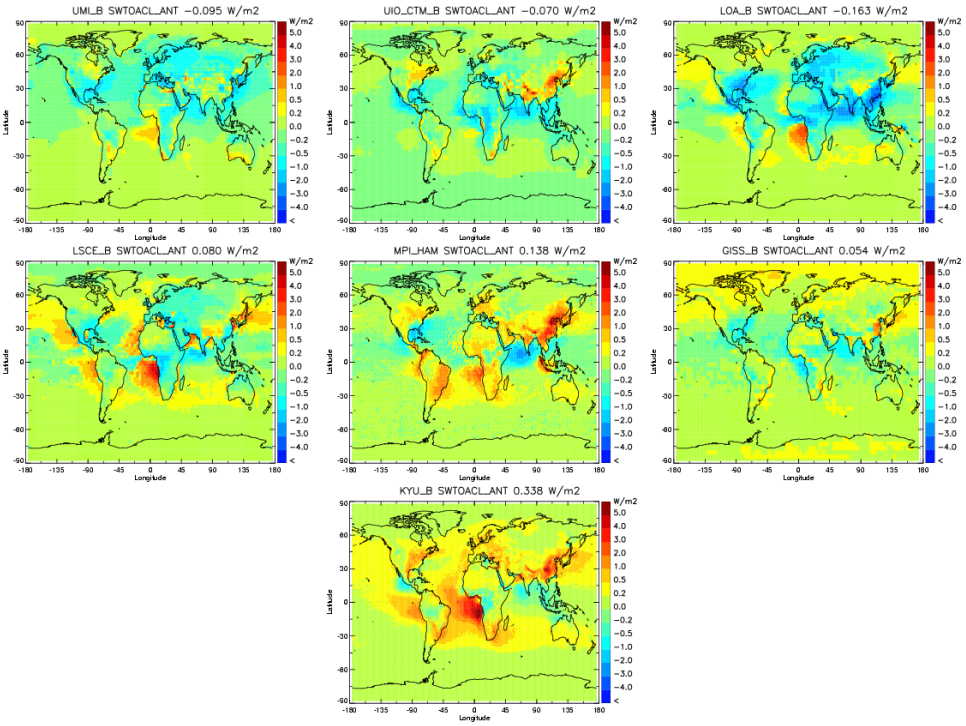

Fig. 6. Same as Fig. 4 but cloud-sky condition total direct aerosol forcing in the AeroCom models.

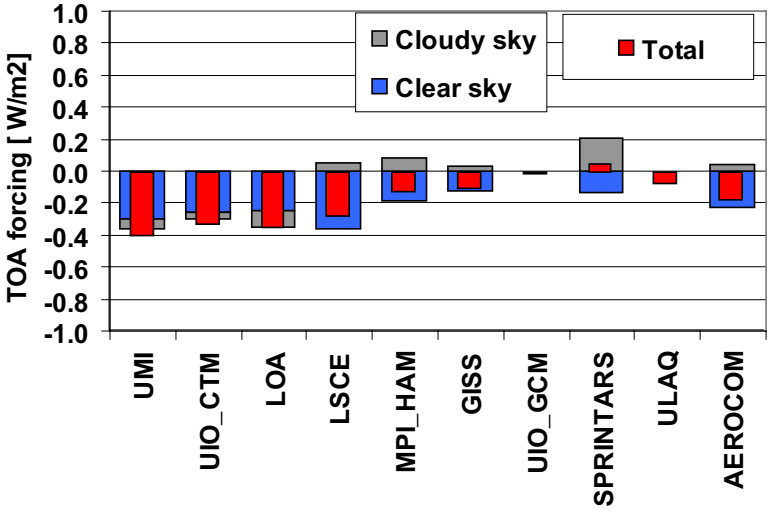

Fig. 7. Total direct aerosol forcing, and contributions from clear-sky and cloud-sky conditions. For the latter clear sky and cloud-sky area fractions are multiplied with the clear sky and cloud-sky forcing values.

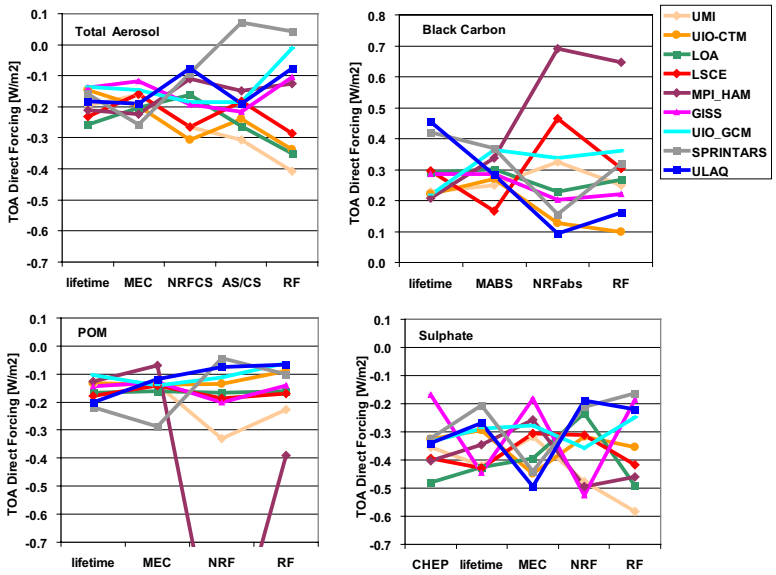

Fig. 8. Partial sensitivity of aerosol forcing to variation in different factors x (see below) of the total anthropogenic aerosol and components in AeroCom models. Shown are recalculated forcings $F_{x,n}=x_n/<x>*<RF>$; with $x_n/<x>$ being the ratio of factor x of model n over its respective AeroCom mean <x>; and with <RF> being the mean AeroCom aerosol or component forcing. For absolute values refer to Tables 2–5. Factors x explanations: "CHEP" ratio of sulphate chemical production over emission of SO2; "lifetime": residence time in the atmosphere; "MEC": Mass extinction coefficient; "MABS": BC aerosol absorption coefficient; "NRF": Normalised radiative forcing per unit optical depth; "NRFabs" Normalised radiative forcing per unit absorption optical depth; "NRFCS": Normalised clear-sky radiative forcing per unit optical depth; "AS/CS": All-sky over clear-sky RF ratio; "RF"-column: represents original total aerosol or aerosol component forcing in each of the AeroCom models.

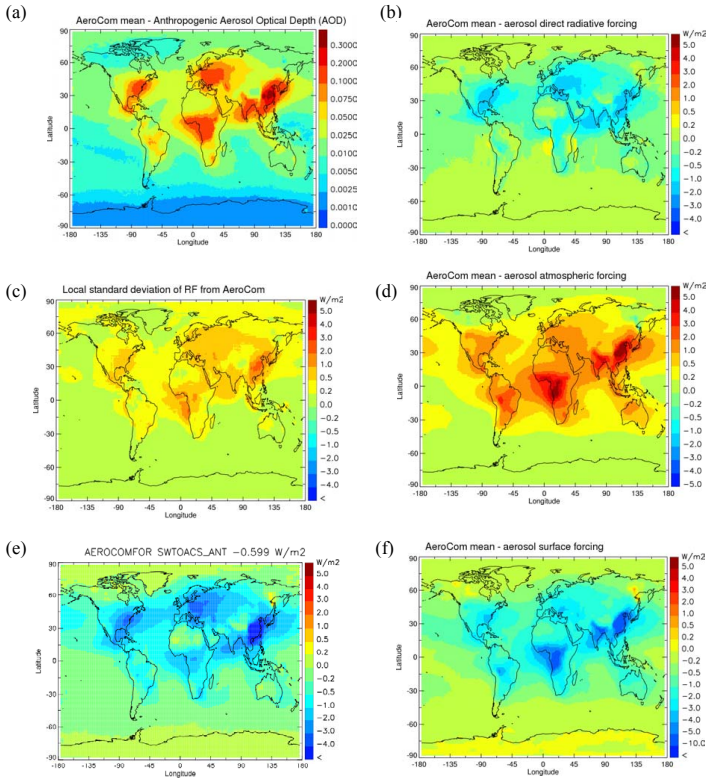

Fig. 9. Mean annual fields derived from the regridded AeroCom model simulations of **(a)** anthropogenic aerosol optical depth; **(b)** radiative forcing **(c)** local standard deviation from 9 models of RF **d)** atmospheric forcing of column; **(e)** clear-sky RF; **(f)** surface forcing. See values in Table 5.